https://dx.doi.org/10.1016/j.envpol.2018.05.042

This is the Pre-Published Version.

Causes of ozone pollution in summer ~~of~~ in Wuhan, Central China

P. Zeng[1,2], X.P. Lyu[2], H. Guo[2*], H.R. Cheng[1**], F. Jiang[3], W.Z. Pan[2], Z.W. Wang[1], S.W. Liang[3], Y.Q. Hu[3]

1. School of Resource and Environmental Sciences, Wuhan University, Wuhan 430072, China

2. Department of Civil and Environmental Engineering, The Hong Kong Polytechnic University, Hong Kong, China

3. International Institute for Earth System Science, Nanjing University, Nanjing 210023, China

4. Wuhan Environment Monitoring Center, Wuhan 430022, China

*Corresponding author. ceguohai@polyu.edu.hk;

**Second corresponding author. chenghr@whu.edu.cn

Abstract

In August 2016, continuous measurements of volatile organic compounds (VOCs) and trace gases were conducted at an urban site in Wuhan. Four high-ozone (O_3) days and twenty-seven non-high-O_3 days were identified according to the China's National Standard Level II (~100 ppb). The occurrence of high-O_3 days was accompanied by tropical cyclones. Much higher concentrations of VOCs and carbon monoxide (CO) were observed on the high-O_3 days (p<0.01). Model simulations revealed that vehicle exhausts were the dominant sources of VOCs, ~~with the~~ contributi~~on of~~ng 45.4 ± 5.2% and 37.3 ± 2.9% during high-O_3 and non-high-O_3 days, respectively. Both vehicle exhausts and stationary combustion made significantly larger contributions to O_3 production on high-O_3 days (p<0.01). Analysis ~~of~~ using a chemical transport model found that local photochemical formation accounted for 74.7 ± 5.8% of the daytime O_3, around twice the regional transport (32.2 ± 5.4%), while the nighttime O_3 was mainly attributable to regional transport (59.1 ± 9.9%). The local O_3 formation was generally limited by VOCs in urban Wuhan. To effectively control O_3 pollution, the reduction ratio of VOCs to NO_x concentrations should not be lower than 0.73, and the most efficient O_3 abatement could be achieved by reducing VOCs from vehicle exhausts. This study contributes~~d~~ to the worldwide database of ~~the~~ O_3-VOC-NO_x

© 2018. This manuscript version is made available under the CC-BY-NC-ND 4.0 license http://creativecommons.org/licenses/by-nc-nd/4.0/

sensitivity research. ~~The~~ Its findings ~~of this study are~~will be helpful ~~to~~ in formulat~~ing~~e and implement~~ing~~ ~~the~~ emission control strategies ~~against~~ for dealing with O_3 pollution in Wuhan.

Keywords: VOCs, Source apportionment, O_3 formation, Vehicle exhausts, Control measures

Capsule: Local formation dominated ~~the~~ daytime O_3, while ~~the~~ nighttime O_3 was attributable to regional transport in Wuhan.

1. Introduction

Over the past decades, tropospheric ozone (O_3) pollution has become a major problem around the world because of its deleterious impact on human health, vegetation, and climate (Krupa and Manning, 1988; Tilton, 1989; Stevenson et al., 2013; Monks et al., 2015). In recent years, the issue of severe O_3 pollution ~~has attracted broad attention~~ in ~~many~~ megacities and fast-developing regions in China has attracted much attention (Wang et al., 2009; Xue et al., 2014; Verstraeten et al., 2015; Gao et al., 2017; Wang et al., 2017). To effectively control ~~the~~ O_3 pollution, it is ~~urgently necessary~~essential to ~~investigate~~ understand the characteristics and formation mechanisms of O_3 pollution in Chinese cities with different energy structures and geographic features, such as Wuhan in Central China.

The global background, intrusion of stratospheric O_3, and photochemical formation are the main sources of tropospheric O_3, among which photochemical formation generally dominates O_3 levels in urban areas (Monks et al., 2015; Wang et al., 2016; Gao et al., 2017; Wang et al., 2017). In ozone chemistry, O_3 is formed through the ~~photolysis of NO_2, following by the~~ combination ~~between~~of an oxygen atom from NO_2 photolysis ~~and~~ with oxygen (O_2) (Logan, 1985; Roelofs and Lelieveld, 1997). Con~~Re~~versely, O_3 reacts with NO, regenerating NO_2. NO, NO_2, and O_3 can reach a photo-equilibrium, which is driven by ~~the~~ oxidative radicals (e.g. OH, HO_2, and RO_2) (Monks, 2005). NO_x plays a dual role~~s~~ in O_3 formation. In ~~the~~ a low NO_x environment, it stimulates O_3 formation, while in a NO_x-rich environment, O_3 is depleted by NO_x mainly due to the titration of NO to O_3 (Wang et al., 2016). The relationship~~s~~ between O_3 and its precursors in these complicated photochemical processes have been well documented in many previous studies. For example, it has been extensively reported that VOCs are the limiting factors of O_3 production in the urban

Formatted: French (France)
Field Code Changed
Formatted: French (France)
Field Code Changed
Formatted: French (France)
Formatted: Not Superscript/ Subscript
Formatted: French (France)
Formatted: French (France)
Field Code Changed

areas of many Chinese cities, ~~spanning~~ from Beijing in the north to Hong Kong in the south (Wang et al., 2010; Lyu et al., 2016b; Xu et al., 2017). However, in ~~the~~ rural or background regions, O_3 formation is generally NO_x-limited due to the relatively low NO_x (high VOCs/NO_x ratio) in the atmosphere (Pan et al., 2015; Xu et al., 2015). ~~The~~ A NO_x-limited regime ~~is~~ has also been observed or ~~/~~simulated in some cities of western China (Xue et al., 2014; Feng et al., 2016). Regardless of the regimes controlling O_3 formation, the responses of O_3 formation to ~~the~~ precursors are generally non-linear, ~~which is~~as has been revealed by ~~the~~ empirical kinetic modeling approach (EKMA) curves (Lin et al., 1988; Jia et al., 2016; Lyu et al., 2016a). In ~~the~~ a VOC-limited regime, alkenes, aromatics, and biogenic VOCs ~~are~~ have been repeatedly confirmed as the main contributors to O_3 production. An et al. (2012) indicated that aromatics and alkenes contributed 73 - 84% to ~~the~~ O_3 production in summer 2008 in Beijing. Han et al. (2013) found that alkenes were the largest contributors to O_3 production (53.3%), followed by aromatics (35.1%) and alkanes (9.2%), in autumn 2009 in Tianjin. Geng et al. (2007) reported that aromatics were the main contributor (79%) to ~~the~~ O_3 production in November 2005 in Shanghai. The sources of VOCs in China ~~were~~ have also been widely investigated ~~in China~~ (Guo et al., 2007; Yuan et al., 2010; Lyu et al., 2016b; Gao et al., 2017). The contributions of different sources to VOCs vary significantly among cities and regions, but ~~the~~ vehicular and industrial emissions are generally the ~~most~~ predominant sources of ambient VOCs in China (see Table S1 for details). For instance, Shao et al. (2016) indicated that in summer 2013 in Nanjing, industry-related sources (52%) ~~was~~ were the largest contributor to VOCs, followed by vehicular emissions (34%) ~~in summer 2013 in Nanjing~~. Yuan et al. (2009) reported that vehicular emissions made the largest contribution to ambient VOCs ~~in~~ at both urban (62%) and rural sites (36%) in 2006 in Beijing. Ling and Guo (2014) found that vehicular-~~-~~related sources, including gasoline exhaust (22%), diesel exhaust (20%), LPG usage (21%), and gasoline evaporation (8%), were the dominant contributors to VOCs in autumn 2010 in Hong Kong.

Wuhan is the largest city in Central China~~,~~; it is located in an area ~~which is~~ dominated by the moist subtropical ~~moist~~ monsoon climate. ~~With~~ Due to rapid industrialization and urbanization, ~~the~~ O_3 pollution has become increasingly severe in Wuhan. Ozone was identified as the main air

Formatted: French (France)
Field Code Changed
Formatted: French (France)
Field Code Changed
Formatted: French (France)
Formatted: French (France)
Formatted: French (France)
Field Code Changed
Formatted: French (France)

pollutant on 44 days in 2015 and on 34 days in 2016 in Wuhan, when the O_3 un-attainment rate [Please clarify "O_3 un-attainment rate": "un-attainment" is not idiomatic, and it is not clear what was not being attained.] was 15.7% and 9.3% according to China's National Ambient Air Quality Standard Level II (200 μg m^{-3}), respectively (accessible at http://www.whepb.gov.cn/hbHjzkgb/19431.jhtml). Higher O_3 values were generally observed in summer, with the a peak concentration of 121 ppbv in 2015 and 116 ppbv in 2016. As such, Wuhan is faces major ing great challenges in for O_3 abatement, just like the other fast-developing cities and regions in China.

This study aimsed to characterize the O_3 pollution during high-O_3 and non-high-O_3 days so as to understand the main causes of high O_3 days in Wuhan. Specifically, tThe concentrations and compositions of VOCs and NO_x were are firstly compared between high-O_3 and non-high-O_3 days. SecondNextly, the a positive matrix factorization (PMF) receptor model coupled with a photochemical box model incorporating the Master Chemical Mechanism (PBM-MCM) was is applied to investigate the major sources and their contributions to ambient VOCs and photochemical O_3 formation during high-O_3 days and non-high-O_3 days. LastlyFinally, the O_3-precursor relationships were are evaluated with using a the approach of relative incremental reactivity (RIR) approach, and a reduction ratio of VOCs/NO_x was is recommended for effective mitigation of O_3 pollution in Wuhan. The outcomes are expected to improve our understanding of photochemical O_3 formation and transport mechanisms for subtropical regions that havewith moist monsoon climates and a complex coupling of meteorology and chemistry. Our results also have implications for other subtropical inland regions around the world.

2. Methodology

2.1 Sampling site

The sampling site is located in the urban area of Wuhan (30.604° N, 114.278° E), which is adjacent (~70 m) to a main traffic road and surrounded by residential and commercial blocks (Fig. 1). The instruments were deployed on the roof of a nine-story building (~25 m a.g.l.), the of Wuhan Research Institute of Environmental Protection.

Formatted: Highlight

Formatted: Highlight

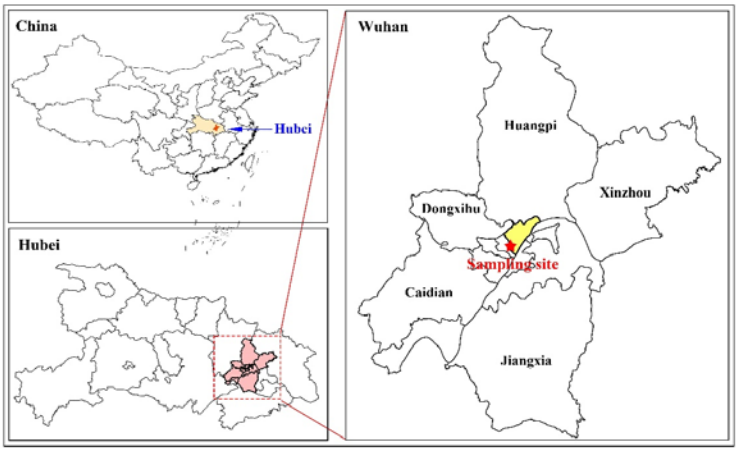

Fig. 1. Geographical location of the sampling site

2.2 Measurement techniques

2.2.1 On-line measurement of ambient VOCs

102 VOCs species, including 58 non-methane hydrocarbons (NMHCs), 31 halocarbons, and 13 oxygenated VOCs (OVOCs), were analyzed using an online gas chromatography-mass spectrometry-flame ionization detector system with one-hour time resolution (GC-MSD-FID, TH-PKU 300B; Tianhong Instrument Co., Ltd., Wuhan). This online system ~~consists of~~has four parts: the~~, i.e.,~~ sampling system, pre-concentrator, GC-MSD-FID system, and data processing system. Ambient air was continuously drawn through a Teflon tube with an inner diameter of 0.76 cm, and a particle filter was connected to the sampling tube inlet to remove ambient particles. The sampling tube inlet was installed at 1~2 m above the rooftop, and the outlet was connected to a PFA-made manifold with a by-pass pump drawing air at a rate of 15 L min^{-1}. ~~When the~~A ~~a~~ir samples were collected and transferred to the pre-concentrator~~,~~ water and carbon dioxide were removed at -80 °C and VOCs were trapped at -150 °C. After preconcentration, the VOCs were desorbed by rapidly heating up the trap to 100 °C, and then introduced into the GC-FID-MSD system (Li et al., 2015; Lyu et al., 2016). The C_2 - C_4 NMHCs were analyzed by the FID, while other compounds were quantified by MSD. The quality assurance and control (QA/QC) ~~is~~ are shown in Text S1.

2.2.2 Monitoring of trace gases other than VOCs and meteorological parameters

Five trace gases (O_3, NO_2, NO, CO, and SO_2) were measured continuously from ~~1~~ August 1 to 31, ~~August~~ 2016, with a one-hour resolution ~~of one hour~~. Trace gases were monitored using ~~the~~ instruments developed by Thermo Environmental Instruments (TEI) Inc. Specifically, O_3 was detected with a commercial UV photometric analyzer (TEI, Model 49i), which has a detection limit of 1.0 ppbv. Nitric oxide (NO) and NO_2 were analyzed by a chemiluminescence trace level analyzer (TEI, Model 42i) with a detection limit of 0.5 ppbv (Geng et al., 2009). A gas filter correlation CO analyzer (TEI, Model 48i) was used to detect ~~the~~ ambient CO. The detection limit of the CO analyzer was 0.04 ppm. Sulfur dioxide (SO_2) was analyzed using a pulse fluorescence analyzer (TEI, Model 43i) with a detection limit of 0.05 ppbv. The QA/QC of trace gases can be found in Text S1. Weather parameters, including temperature, relative humidity, pressure, wind speed, and wind direction, were also monitored at the site ~~in~~ with ~~hourly~~ a one-hour resolution by the integrated sensor suite (Vantage Pro TM & Vantage Pro 2 Plus TM Weather Stations, Davis Instruments).

In this study, high-O_3 days were defined as those when the highest hourly O_3 concentration exceeded ~~the~~ China's National Ambient Air Quality Standard Level II of 200 μg m^3 (~100 ppbv) (accessible at http://english.mep.gov.cn/Resources/standards/Air_Environment/quality_standard1/201605/t20160511_337502.shtml). Otherwise, the sampling days were denoted as non-high-O_3 days. As such, four~~4~~ high-O_3 days~~,~~ (August ~~i.e.,~~ 1, 17, 24, and 30~~)~~ ~~August,~~ were captured during the entire sampling period.

2.3 Model description

2.3.1. PMF model

The U.S. Environmental Protection Agency (EPA) Positive Matrix Factorization (PMF, version 5.0) model was applied to identify the sources of ambient VOCs and to quantify their contributions to VOCs. PMF is a multivariate factor analysis tool that decomposes a matrix of speciated sample data into two matrices: factor contributions (G) and factor profiles (F). Here, ~~the~~ "factor contribution" means the contribution of a source to the total measured VOC concentration in a

sample, while "factor profile" indicates the percentages of individual VOC species in the total measured VOC concentration in a sample. To ascribe the concentrations of *m* chemical species in *n* samples to *p* independent sources, the receptor model can be generally expressed as follows (Eq. 1):

$$x_{ij} = \sum_{k=1}^{p} g_{ik} f_{kj} + e_{ij} \qquad \text{(Eq. 1)}$$

where x_{ij} (unit: ppbv) is the concentration of the *j*th species in the *i*th sample, g_{ik} (unit: ppbv) is the contribution of the *k*th source to the *i*th sample, f_{kj} is the fraction of *j*th species in *k*th source, and e_{ij} is the residual for the *i*th sample of the *j*th species.

The factor profiles were derived based on the principle that the objective function Q ~~had~~ should have the lowest value, as shown in Eq. (2) (Paatero and Tapper, 1994; Paatero, 1997). In addition, the profiles should have the best interpretability.

$$Q = \sum_{i=1}^{n} \sum_{j=1}^{m} \left[\frac{e_{ij}}{u_{ij}}\right]^2 \qquad \text{(Eq. 2)}$$

where u_{ij} is the uncertainty of the *i*th species in the *j*th sample. The function value, Q(robust), was calculated ~~by~~ using the model ~~through~~ by excluding the points with ~~the~~ uncertainty-scaled residuals greater than 4. The profile with the lowest value of Q(robust) was selected as the optimum solution.

In this study, speciated VOCs including 20 NMHCs, chloromethane, and ~~trichlorethylene~~trichloroethylene from 565 samples (m) were input into the PMF model. The 22 species (n) were selected because most of them are tracers of different sources. ~~Since~~Because accuracies in measurements for all species were <10% (Table S1), we used 10% as input to represent the uncertainty of each species in each sample in the model. Different numbers of factors ~~was~~ were tested, and an optimum solution was determined based on ~~a~~ good fit to the observed data and the most meaningful results. Eventually, seven factors (p) were extracted from the PMF model simulation.

2.3.2 PBM-MCM model

A zero-dimension Lagrangian photochemical box model incorporating a Master Chemical Mechanism (PBM-MCM) was applied to investigate ~~the~~ in situ photochemical O_3 formation in

Wuhan in August 2016. This model simulates the complex photochemistry within a well-mixed boundary layer air parcel, including 5,900 species and 16,500 reactions. All ~~the~~ air pollutants were assumed to be well mixed in the atmospheric boundary layer defined by the model. It should be noted that ~~the~~ vertical and horizontal dispersions were not considered in the model. ~~The~~ This model was described in detail~~s~~ by Lam et al. (2013) and its reliability has been repeatedly confirmed ~~reliable~~ in previous studies (Cheng et al., 2013; Ling et al., 2014; Lyu et al., 2016b). In this study, the observed hourly values of 52 VOCs and four~~4~~ trace gases (NO_2, NO, SO_2, and CO), ~~as well as~~in addition to temperature and relative humidity, between 00:00 local standard time (LST) and 23:00 LST were used to construct the model. The photolysis rates of different chemicals in the model were parameterized using the photon flux determined from the Tropospheric Ultraviolet and Visible Radiation (TUVv5) model (Lam et al., 2013). The simulations of daytime hours (07:00 - 19:00 LST) were conducted for the entire sampling period except for the rainy days, and the model output was the simulated hourly mixing ratios of O_3. The in situ O_3 production, the O_3-NO_x-VOCs relationship, and the control strategies of O_3 were all simulated using the PBM-MCM model. ~~The~~ Ddetail~~sed descriptions~~ of the modeling results ~~were~~ are shown in section 3.2.2 and section 3.4.

In addition to the simulation of O_3 production, the PBM-MCM model was applied to investigate ~~the~~ O_3-precursor relationships ~~through~~ by examining the relative incremental reactivity (RIR~~s~~) of O_3 precursors. The RIR is the percentage change in daytime O_3 production per percent change in precursor. ~~The~~ O_3 precursors were divided into four groups~~, i.e.,~~ anthropogenic VOCs (AVOCs), BVOCs, CO, and NO_x. A positive RIR ~~of~~ for a given precursor means that reducing emissions of this precursor will significantly reduce O_3 production, whereas a negative RIR indicates the opposite effect, i.e., cutting emissions of the precursor will enhance O_3 production. In general, the RIRs of VOCs are positive, while both positive and negative RIRs are commonly seen for NO_x due to its dual role in O_3 chemistry. The VOC-limited (VOC-sensitive) regime is indicated by the positive RIRs of VOCs and negative RIRs of NO_x. Otherwise, O_3 formation is limited by (sensitive to) NO_x or both VOCs and NO_x when the RIR of NO_x is positive.

–The RIR for precursor X at site "s" is calculated using Eq. 3 (Cardelino and Chameides, 1995):

$$RIR^{S}(X) = \frac{\left[P^{S}_{O_3\text{-}NO}(X) - P^{S}_{O_3\text{-}NO}(X-\Delta X)\right]/P^{S}_{O_3\text{-}NO}(X)}{\Delta S(X)/S(X)} \quad \text{(Eq. 3)}$$

where X represents a specific precursor (i.e. VOCs, NOx, or CO); the superscript "S" is used to denote the specific site where the measurements were made; S(X) is the measured mixing ratio of species X (ppbv); ΔS(X) is the hypothetical change in the mixing ratio of X, which is artificially set ~~as~~ at 10%; $P^{S}_{O_3\text{-}NO}(X)$ represents the simulated O_3 production in the base run constructed with the observed concentrations of all ~~the~~ O_3 precursors, including ~~the~~ species X. $P^{S}_{O_3\text{-}NO}(X-\Delta X)$ is the simulated O_3 production in the constrained run with 10% reduction of species X (Ling et al., 2013; Wang et al., 2018; Xu et al., 2017), while the concentrations of other species remain~~ed~~ unchanged. The titration of O_3 by NO was considered in both runs. Then, the average RIR value ($\overline{RIR}$) for the species X over multiple sampling days was calculated using Eq. (4)~~.~~, w~~W~~here NS means the number of days simulated.

$$\overline{RIR} = \frac{\sum_{1}^{NS}\left[RIR^{S}(X)P^{S}_{O_3\text{-}NO}(X)\right]}{\sum_{1}^{NS}P^{S}_{O_3\text{-}NO}(X)} \quad \text{(Eq. 4)}$$

2.3.3 WRF-CMAQ model

The U.S. EPA Community Multiscale Air Quality (CMAQ) model with the Carbon Bond 05 (CB05) chemical mechanism was applied to simulate ~~the~~ O_3 concentrations during ~~the~~ high-O_3 days. CMAQ is a three-dimensional atmospheric chemistry and transport modeling system~~;~~, ~~and~~ more details ~~about the CMAQ model~~ can be found at http://cmascenter.org/cmaq/. In this study, CMAQ was driven by the meteorological fields from the Weather Research and Forecasting (WRF) model, which is one of the most ~~currently~~ commonly used~~available~~ models ~~to apply~~ for both forecasting and atmospheric research across scales ranging from meters to thousands of kilometers. The simulation period was 00:00 LST, August 13, 2016, ~~from 00:00 LST 13 August 2016~~ to 23:00 LST, August 18, 2016, ~~23:00 LST 18 August 2016~~ when continuously high O_3 values were observed, with the highest hourly O_3 of 133.9 ppbv on ~~17~~ August 17 (Fig. S1). The purpose ~~to~~ of running the model simulations for ~~the~~ six~~6~~ consecutive days was to ensure that the modeling could

achieve ~~the~~ a balance of ~~the~~ intermediates (e.g. radicals) and reduce ~~the~~ integration error in numerical calculations (~~-~~Jiang et al., 2008; Pan et al., 2015; Chen et al., 2018). Two nested domains were defined in the WRF modeling, and the corresponding grid spacings were 27 km and 9 km, ~~receptivity~~respectively. The outer domain (DM1, 27 km) covered most ~~territory~~ of China, and the second domain (DM2, 9 km) included most cities in eastern Hubei Province, and some parts of Anhui, Henan, and Jiangxi Provinces. Vertically, there were 31 sigma levels, with the top pressure fixed at 100 hPa. The meteorological parameters were well considered by the model (Jiang et al., 2010). The anthropogenic emission inventory developed by Tsinghua University based on figures for ~~the year of~~ 2010 was applied for this study, which includes monthly anthropogenic emissions of SO_2, NO_x, CO, ammonia (NH_3), $PM_{2.5}$, PM_{coarse}, black carbon (BC), organic carbon (OC), and non-methane volatile organic compounds (NMVOCs). The data ~~has~~ have a horizontal resolution of 0.25° × 0.25°. More details are given by He (2012). The biogenic emissions were calculated offline using the Model of Emissions of Gases and Aerosols from Nature (MEGAN, version 2.04) (Guenther et al., 2006). These modeling systems have been successfully used in previous O_3 simulations by Jiang et al. (2010) and Wang et al. (2015).

Formatted: Font: Not Italic

3 Results and discussion

3.1 Characteristics of meteorological parameters and air pollutants

Table S2 shows the descriptive statistics of meteorological parameters on high-O_3 and non-high-O_3 days. The occurrence of high-O_3 days was associated with high temperature, low wind speed, and low relative humidity. Fig. S3 presents the distributions of mean sea level (MSL) pressure and wind fields averaged over high-O_3 days and non-high-O_3 days in East Asia. It ~~is shown~~indicates that the high-O_3 days were all related to tropical cyclones. ~~This is because~~This relation exists ~~because reason is that~~ Wuhan ~~was~~ is located on the periphery of ~~the~~ tropical cyclones, where relatively high pressure and subsiding air ~~were~~ are formed, causing O_3 accumulation. In addition, ~~the~~ east to north winds induced by the tropical cyclones also brought ~~the~~ polluted air masses from East China and North China to Wuhan on these days. A detailed discussion is given in Text S2 in the Supplement.

The time series of observed O_3 concentrations in Wuhan in August 2016 is shown in Fig. S1. ~~According to~~ Based on the definition of a high-O_3 day, August 1, 17, 24, and 30 ~~August~~ were defined as high-O_3 days during the sampling period. Table S3 shows the statistical descriptions of air pollutants on high-O_3 and non-high-O_3 days. During high-O_3 days, the O_3 mixing ratio was 61.2 ± 7.4 ppbv, about 40% higher than ~~that (42.3 ± 2.0 ppbv)~~ on non-high-O_3 days ~~(~~(42.3 ± 2.0 ppbv; p<0.01). The mixing ratios of O_3 precursors, i.e., CO and total VOCs (TVOCs) representing the sum of mixing ratios of 102 VOC species, were 987.8 ± 95.4 and 43.9 ± 3.8 ppbv on high-O_3 days, respectively, about 37% and 33% higher than ~~those~~ on non-high-O_3 days (p<0.01)~~,~~ ~~respectively~~. However, the levels of NO and NO_2 were comparable between high-O_3 and non-high-O_3 days (the differences < 2 ppbv, p>0.05). Previous studies indicated that O_3 formation is generally limited by VOCs and suppressed by NO_x in urban areas (Wang et al., 2008; Ling et al., 2013; Lyu et al., 2016b). Hence, the more abundant TVOCs and CO during high-O_3 days and comparable NO_x values between high-O_3 and non-high-O_3 days might indicate the significant contribution of local photochemical reactions to O_3 formation.

Fig. S2 shows the diurnal variations of O_3, NO_x, and *m*,*p*-xylene/ethylbenzene ratio on high-O_3 and non-high-O_3 days. The observed O_3 generally peaked in the afternoon, and had relatively low concentrations from midnight to the early morning on both high-O_3 and non-high-O_3 days. A trough of O_3 appeared at about 08:00 LST, which was likely caused by ~~the~~ enhanced NO titration due to ~~the~~ increased vehicular emissions of NO ~~in~~ during morning rush hour~~s~~ (So and Wang, 2003). In fact, the diurnal variation of NO_x was opposite to that of O_3~~:~~. ~~Namely, the~~ high levels of NO_x appeared in the morning and evening when O_3 was relatively low, and the increase of O_3 from 09:00 to 15:00 corresponded to the decrease of NO_x. The opposite diurnal patterns between O_3 and NO_x indicated that O_3 formation in Wuhan was in a VOC-limited (NO_x-suppressed) regime. The diurnal trend of *m*,*p*-xylene/ethylbenzene was also negatively correlated to O_3. ~~Since~~Because *m*,*p*-xylene is more reactive than ethylbenzene, the ratios of *m*,*p*-xylene/ethylbenzene ~~would~~ decreased when photochemical reaction occurred. Indeed, the lowest ratios were observed in early afternoon when O_3 peaked, while higher ratios were found in the morning and late afternoon, indicating fresh

Field Code Changed
Formatted: French (France)
Formatted: French (France)
Formatted: Not Superscript/ Subscript

vehicular exhaust emissions and relatively weak photochemical consumption of VOCs.

Fig. 2 shows the diurnal variations of TVOCs, ethene, propane, toluene, and isoprene on O_3 and non-high O_3 days. In general, the patterns between high-O_3 and non-high-O_3 days for TVOCs and individual VOC species were similar, except for the magnitude. Moreover, TVOCs showed the same trend as ethene, propane, and toluene~~. Namely,~~ a bimodal structure was observed with the first peak in the morning and the second one in late afternoon, likely due to vehicular exhausts during rush hour~~s~~ and strong photochemical reactions at noon and in early afternoon. Clearly, the mixing ratios of TVOCs, ethene, propane, and toluene during high-O_3 days were about 37%, 31%, 48%, and 30% higher than ~~those~~ during non-high-O_3 days (p<0.01). It ~~was~~ is unlikely that the local emissions of these air pollutants changed substantially between high-O_3 and non-high-O_3 days. ~~Since~~Because more O_3 precursors were usually consumed by intensive photochemical reactions on high-O_3 days, the more abundant O_3 precursors on high-O_3 days might indicate poor dispersion and dilution of air pollutants. Conversely, higher levels of isoprene were observed during daytime than ~~that~~ at night, suggesting that biogenic emission (BVOCs) of isoprene was more enhanced than its photochemical oxidation and dispersion ~~at~~ during daytime hours. Isoprene is often used as a tracer of biogenic sources, as it is the most abundant compound in vegetation emissions (Guenther et al., 2006; Sharkey et al., 2008). Mixing ratios of isoprene were comparable (p>0.05) on both high-O_3 and non-high-O_3 days, indicating that there was no significant difference in ~~the~~ biogenic emission~~s had no significant difference~~ between the two scenarios.

Formatted: Not Highlight

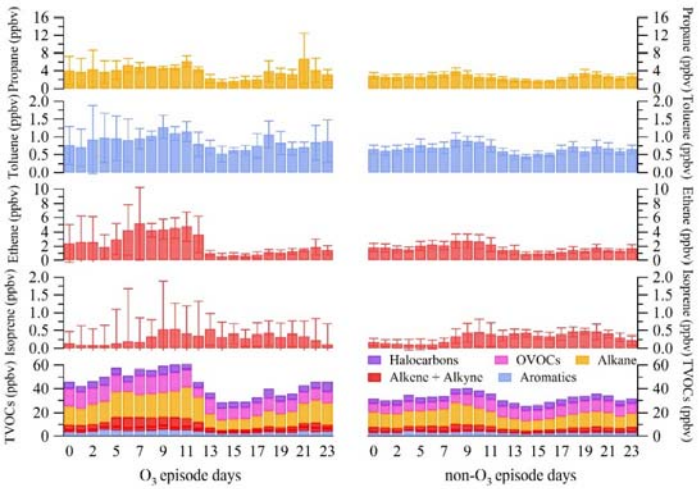

Fig. 2. Average diurnal patterns of grouped VOCs on high-O_3 days (78 samples) and non-high-O_3 days (487 samples)

3.2 Source~~s~~ apportionment of ambient VOCs

3.2.1 Source contribution to VOCs

Seven factors were identified by the PMF to best describe the sources of ambient VOCs~~:~~, ~~i.e.,~~ gasoline exhausts, diesel and compressed natural gas (CNG) exhausts, stationary combustion, the petrochemical industry, solvent usage in painting, asphalt application, and biogenic VOCs (BVOCs) (see Text S3 and Fig. S4 in the supplement for further description). Table 1 lists the source contributions to the total mixing ratios of VOCs ~~applied~~ used for~~in~~ source apportionment on high-O_3 days and non-high-O_3 days, in the forms of mixing ratio and percentage contribution. Not~~ice~~ably, ~~the~~ vehicle emissions, including gasoline exhaust, and diesel and CNG exhausts, were the dominant sources of VOCs, with ~~the~~ total contributions of 45.4 ± 5.2% (11.0 ± 2.1 ppbv) and 37.3 ± 2.9% (7.1 ± 1.0 ppbv) during high-O_3 and non-high-O_3 days, respectively. The contribution of vehicular exhausts to VOCs in this study was comparable to ~~those~~ that found~~obtained~~ at an urban site in Hong Kong (Ling and Guo, 2014), while lower than ~~that~~ in Beijing (Liu et al., 2005). ~~Besides~~In addition, stationary combustion was ~~also~~ an important contributor to ambient VOCs, with ~~the~~ a contribution of 31.5 ± 4.5% (5.6 ± 0.6 ppbv) during high-O_3 days and 36.5 ± 2.7% (4.9

± 0.3 ppbv) during non-high-O_3 days. This finding was is not unreasonable, in view of the considerable coal consumption in Wuhan (more than 17 million tons in 2015) and intensive burning of biomass (e.g. crop residues) burning in and around Wuhan (Lyu et al., 2016).

In comparison, VOCs emitted from diesel and CNG exhausts and solvent usage in painting on high-O_3 days were much higher than those during non-high-O_3 days (p<0.01). However, gasoline exhaust, asphalt application, stationary combustion, and BVOCs made comparable contributions to VOCs between high-O_3 and non-high-O_3 days (p>0.05). In addition, VOCs attributable to the petrochemical industry was were even lower during high-O_3 days (p<0.01). However, sincebecause the reactivity of VOC species in O_3 formation varies in over a wide range (Carter, 1994), we could not conclude that the sources with higher contributions to VOCs (vehicle exhausts, stationary combustion, and solvent usage) were responsible for the occurrence of high-O_3 days. In other words, further investigation was needed into the contributions of VOC sources to O_3 production needed further investigation.

Table 1 Source contributions to VOCs on high-O_3 days and non-high-O_3 days (mean ± 95% confidence interval)

	Mixing ratios (ppbv)		Contribution (%)	
	High-O_3 days	Non-high-O_3 days	High-O_3 days	Non-high-O_3 days
Gasoline exhaust	4.7 ± 0.9	3.7 ± 0.5	23.0 ± 4.0	20.9 ± 1.9
Diesel and CNG exhausts	6.3 ± 1.6	3.4 ± 0.7	22.4 ± 4.1	16.4 ± 2.2
(Vehicle exhausts)	(11.0 ± 2.1)	(7.1 ± 1.0)	(45.4 ± 5.2)	(37.3 ± 2.9)
BVOCs	0.5 ± 0.1	0.5 ± 0.1	3.0 ± 0.6	3.8 ± 0.5
Stationary combustion	5.6 ± 0.6	4.9 ± 0.3	31.5 ± 4.5	36.5 ± 2.7
Asphalt application	1.5 ± 0.6	1.6 ± 0.4	7.8 ± 2.5	9.7 ± 2.2
Solvent usage in painting	1.5 ± 0.3	0.8 ± 0.1	7.9 ± 1.2	5.3 ± 0.6
Petrochemical	0.9 ± 0.2	1.1 ± 0.1	4.4 ± 0.8	7.4 ± 0.7

industry

3.2.2 Source contributions to O_3 production

To further understand the contributions of different VOC~~s~~ sources to O_3 formation, the in situ production of O_3 was simulated ~~by~~ using the PBM-MCM model. ~~Since~~ Because ~~the~~ photolysis rates could not be well calibrated on rainy days and wet deposition was not considered in the model, there ~~generally~~ were often major~~great~~ discrepancies between ~~the~~ observed and simulated O_3 on rainy days. Therefore, ~~the~~ days with precipitation (in total 10 days) were excluded in the O_3 simulation. In addition, the instruments were maintained on some days to guarantee ~~the~~ data quality. These days were also ~~not~~ omitted from the~~included in~~ O_3 simulation. Fig. S5 in the supplement shows the model validation results. ~~It was found that~~These indicate that ~~that~~ the PBM-MCM model well reproduced the levels and diurnal trends of O_3, implying that O_3 on these days was mainly locally formed. However, O_3 was only simulated in this study ~~at~~ for daytime hours (07:00 - 19:00 LST)~~ in this study~~. In fact, O_3 simulation by a chemical transport model in the same period indicated that while local formation was responsible for daytime O_3, regional transport elevated nocturnal O_3 (more details ~~shown~~ are given in 3.3).

Two scenarios for O_3 simulation (~~, i.e.~~ a base scenario and a constrained scenario)~~,~~ were run to investigate the contribution of a specific VOC source to ~~the~~ O_3 production. The observed VOCs were used to construct the base scenario, while in the constrained scenario VOCs emitted from an individual specific source were deducted. The difference in simulated O_3 between the base and constrained scenarios was the net O_3 production of the specific source. In this way, the contribution of each VOC source to O_3 production was obtained. It is noteworthy that the data on the four~~4~~ high-O_3 days were included for source apportionment. ~~Since~~Because species with high reactivity participate more in photochemical reactions during high-O_3 days, their contributions to O_3 production were ~~partly~~ somewhat underestimated.

Table 2 summarizes the contributions of VOC sources to O_3 production on high-O_3 days and non-high-O_3 days. It was found that vehicle exhausts (exhausts from gasoline-, diesel- and CNG-

fueled vehicles) made the largest contribution to O_3 production, with 34.0 ± 1.4% (13.9 ± 2.2 ppbv) during high-O_3 days and 29.5 ± 0.7% (8.3 ± 0.9 ppbv) during non-high-O_3 days. However, compared to their contributions to VOCs (45.4 ± 5.2% during high-O_3 days, and 37.3 ± 2.9% during non-high-O_3 days; $p<0.01$) the contribution of vehicle exhausts to O_3 production was lower ($p<0.01$). ~~On the contrary~~In contrast, the contributions to O_3 production of the petrochemical industry, solvent usage in painting, and BVOCs were obviously higher than their contributions to VOCs ($p<0.01$). This discrepancy might be caused by the source-specific compositions of VOCs and the different reactivity of VOCs in O_3 formation. More importantly, we noticed that O_3 produced by vehicle exhausts (the sum of exhausts from gasoline-, diesel- and CNG-fueled vehicles) and stationary combustion all increased significantly during high-O_3 days ($p<0.05$). ~~Particularly~~In particular, O_3 produced by VOCs from diesel and CNG exhausts increased from 13.7 ± 0.6% (3.9 ± 0.4 ppbv) during non-high-O_3 days to 19.2 ± 1.3% (7.8 ± 1.3 ppbv) during high-O_3 days. This finding implies~~d~~ that emission of VOCs from diesel and CNG exhausts was the~~a~~ main culprit ~~of~~ for ~~the~~ elevated O_3 ~~during~~ on high-O_3 days.

Table 2 Source contributions to O_3 production on high-O_3 days and non-high-O_3 days (mean ± 95% confidence interval)

	Net O_3 increment (ppbv)		Contribution (%)	
	High-O_3 days	Non-high-O_3 days	High-O_3 days	Non-high-O_3 days
Gasoline exhaust	6.1 ± 0.9	4.5 ± 0.4	14.8 ± 0.3	15.8 ± 0.5
Diesel and CNG exhausts	7.8 ± 1.3	3.8 ± 0.4	19.2 ± 1.3	13.7 ± 0.6
(Vehicle exhausts)	(13.8 ± 2.2)	(8.3 ± 0.8)	(34.0 ± 1.4)	(29.5 ± 0.7)
BVOCs	6.9 ± 1.1	6.0 ± 0.8	16.7 ± 0.8	20.3 ± 1.1
Stationary combustion	5.3 ± 0.7	3.8 ± 0.4	13.3 ± 0.2	12.7 ± 0.3
Asphalt application	3.3 ± 0.5	2.7 ± 0.4	8.9 ± 1.1	8.5 ± 0.9
Solvent usage in painting	5.9 ± 0.9	4.8 ± 0.5	14.6 ± 0.5	16.4 ± 0.8
Petrochemical industry	4.9 ± 0.7	3.8 ± 0.4	12.5 ± 0.5	12.8 ± 0.3

3.3 Contributions of local formation and regional transport to O_3 levels

To understand the causes of high-O_3 days in Wuhan during the sampling period, the local formation and regional transport of O_3 during the continuous sunny days from August 13 ~~August~~ to 18 ~~August~~ were simulated as a case study ~~with~~ using the WRF-CMAQ model ~~as a case study~~. One of the high-O_3 days ~~(17 August)~~ discussed in section 3.1.2 (August 17) was involved. This case was selected to represent the general characteristics of high-O_3 days during the sampling period, as all the high-O_3 days occurred under similar meteorological conditions (see section 3.1.2). The processes influencing O_3 concentration, i.e. advection and diffusion in ~~both~~ the horizontal and vertical directions, ~~the~~ dry deposition, and chemical reactions, were fully considered in the WRF-CMAQ model. The model configurations were consistent with those described in Jiang et al. (2010). Figure 4 shows the hourly variations of the simulated and observed O_3 through August 13 to 18, 2016, in Wuhan. The model well reproduced the observed O_3 in both magnitude and diurnal pattern, with ~~the~~ an index of agreement of 0.79 (Willmott, 1981).

It is noteworthy that~~,~~ the WRF-CMAQ overestimated O_3 on August 15-16 ~~August~~, but underestimated O_3 on August 13, 17, and 18 ~~August~~ (Figure 4). The PBM-MCM model overestimated O_3 on August 17, 19, 24, and 31 ~~August~~ (Figure S5). Despite the discrepancies, the modeling results were acceptable, in view of the uncertainties inherent in model simulations. For the WRF-CMAQ model, the uncertainty mainly derives from the uncertainty of the emission inventory and the carbon bond chemical mechanisms. Though the PBM-MCM model is near-explicit in chemical mechanisms, it does not consider the physical processes. Therefore, ~~it is expected that~~ some differences ~~exist~~ can be expected between the observed O_3 and simulated O_3 ~~by~~ for both models. In fact, this discrepancy is common in almost all ~~the~~ studies ~~using~~ that use these chemical transport models and box models (e.g., Gao et al., 2016; Wang et al., 2017; Chen et al., 2018).

Formatted: Font: Not Italic

Field Code Changed

Formatted: French (France)

Formatted: French (France)

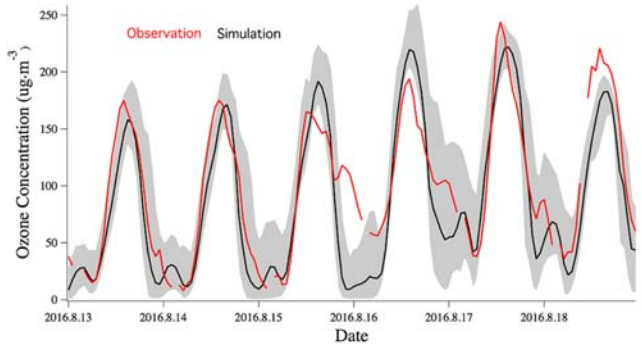

Fig. 4 Time series of simulated and observed O_3 concentrations in Wuhan from 00:00 LST, August 13 ~~August~~ to 23:00 LST, August 18, ~~August~~ 2016. The grey area defines the lowest and highest simulated O_3 at eight~~8~~ air quality monitoring stations (AQMSs) surrounding the sampling site. The AQMSs are managed by the China National Environmental Monitoring Centre.

~~Furthermore, t~~The contributions of different processes to O_3 are summarized in Table 3. Overall, ~~the~~ horizontal advection (-1.3 ± 7.0 ppbv) and diffusion (-0.1 ± 0.02 ppbv) made negative contributions to O_3 mixing ratios. In addition, 3.4 ± 0.6 ppbv of O_3 was removed through dry deposition. In contrast, O_3 was elevated by 3.9 ± 7.5 and 14.2 ± 1.2 ppbv due to ~~the~~ vertical advection and diffusion, respectively. As the largest contributor to O_3, chemical reactions built up the O_3 mixing ratio by 42.3 ± 6.1 ppbv. It is noteworthy that the chemical reactions indicated the process of local O_3 formation. ~~Since~~Because advection and diffusion generally represent the transport of air pollutants, the sum of horizontal and vertical advection/diffusion is referred to hereafter as regional transport ~~hereafter~~ (Jiang et al., 2010; Li et al., 2012; Chen et al., 2018). ~~As a result, r~~Regional transport, local photochemical formation, and dry deposition accounted for 44.4 ± 5.8%, 60.2 ± 6.1% and -4.6 ± 0.5% of the total simulated O_3, respectively. More specifically, the contribution of regional transport (59.1 ± 9.9%) to nighttime O_3 predominated over local formation (42.7 ± 10.1%) (20:00 - 06:00 LST), while daytime O_3 was mainly derived from ~~the~~ local

Formatted: Not Superscript/ Subscript

photochemical formation (74.7 ± 5.8%), about twice the regional transport (32.2 ± 5.4%). ~~It~~ ~~T~~therefore, it would seem ~~was concluded~~ that the high daytime O_3 on high-O_3 days in Wuhan ~~was~~ is primarily attributable to local formation, while regional transport from the east made significant contributions to ~~the~~ nocturnal O_3. In fact, compared to the same time slots on other days, the observed nighttime O_3 increased by 4~~-~~-12 ppbv ~~-~~on August 15~~-~~-17 ~~August~~ (Figure 4), in contrast to ~~the~~ limited nocturnal O_3 production from photochemical reactions and the consumption of O_3 by some substances (e.g. NO and alkenes). As such, the increase of nocturnal O_3 on these days ~~was~~ is most likely attributable to regional transport, consistent with the modeling results.

Formatted: Font: Not Italic

Table 3 Factor contributions to the simulated O_3 during August 13-18, 2016, in Wuhan (Unit: ppbv).

	Average ± 95% Confidence Interval	Maximum	Minimum	Standard deviation
Horizontal advection	-1.3 ± 7.0	125.0	-111.5	42.7
Vertical advection	3.9 ± 7.5	127.8	-128.3	45.5
Horizontal diffusion	-0.1 ± 0.02	0.1	-0.4	0.1
Vertical diffusion	14.2 ± 1.2	36.6	1.5	7.5
Dry deposition	-3.4 ± 0.6	-0.01	-10.9	3.4
Chemical reactions	42.3 ± 6.1	130.5	-8.0	36.9

3.4 Implications for ~~on~~ control strategies

To understand ~~the~~ O_3 formation mechanisms, the relationships between O_3 and its precursors were explored using the PBM-MCM model. ~~The~~ O_3 precursors were divided into four groups, namely ~~i.e.~~ anthropogenic volatile organic compounds (AVOCs), BVOCs, CO, and NO_x~~;~~ ~~then~~ their RIR values were calculated using Eq. 3. According to previous studies (Zhang et al., 2006; Lyu et al., 2016b; Wang et al., 2018), the positive RIR value of VOCs and negative RIR value of NO_x indicate~~s~~ VOCs-limited O_3 production in the study area, while the negative RIR value of VOCs and positive RIR value of NO_x means that production is NO_x-limited. Fig. S6 shows the mean RIR values of O_3 precursors over the high-O_3 and non-high-O_3 days. It ~~was found~~indicates

that the average RIR values of VOCs (AVOCs and BVOCs) were positive, while RIR for NO_x was negative, indicating that O_3 formation was limited by VOCs at this site on both high-O_3 days and non-high-O_3 days. ~~This means~~ The implication is that cutting VOCs could reduce O_3 production, while reducing NO_x would lead to O_3 increase. ~~The~~ A VOC-limited regime was also identified in rural areas of Delhi, India (Kumar et al., 2017), and in urban and suburban Hong Kong (Lyu et al., 2016b). However, Lin et al. (2017) indicated that ~~the~~ summertime O_3 pollution in the southeastern U.S. was alleviated by controlling NO_x emissions, indicating ~~the~~ a NO_x-limited regime in O_3 formation. Jin et al. (2017)~~It also found was also revealed~~ that O_3 production became increasingly sensitive to NO_x in mid-latitude megacities in the northern h~~H~~emisphere (e.g., New York, London, and Seoul) between 2005 and 2015 ~~(Jin et al., 2017)~~. It should be noted that a recent study (McDonald et al., 2018) pointed out the underestimation of VOC~~s~~ emissions from ~~the~~ volatile chemical products in industrialized cities in the U.S., meaning that the current understandings of O_3 formation mechanisms based on ~~the~~ pre-existing emission inventories might need further verification~~s~~. To sum up, ~~the~~ O_3-VOC-NO_x sensitivity should be investigated case by case. This study expand~~ed~~ the worldwide database of ~~the~~ O_3-VOC-NO_x sensitivity to include the situation in developing regions, where NO_x ~~was~~ is ~~on~~ at high levels and might continue to increase if no stringent control strategies ~~were~~ are ~~taken~~ put in place (Jin et al., 2017).

Formatted: Not Highlight

Formatted: Not Highlight

Further, the RIR of AVOCs was much higher than that of BVOCs. ~~Namely~~Thus, O_3 formation was more sensitive to AVOCs, which should ~~thus~~ be ~~more focused~~focused on in O_3 abatement. In addition, relatively high average RIR value was found for CO, indicating that CO had a positive impact on O_3 formation in Wuhan, in contrast to the findings of Wang et al. (2017), who reported that the RIR value of BVOCs was much higher than CO in summer in Hong Kong.

To further investigate the role of NO_x in O_3 chemistry, ~~the~~ O_3 productions with different levels of NO_x were simulated using the PBM-MCM model. Table S5 shows the mean net O_3 production in the base case with the observed NO_x and in the constrained cases with NO_x ~~being~~ reduced by 10%, 20%, 40%, 60%, 80%, 90%, 95%, and 98%. The observed VOCs were applied to all the cases without any reduction. It was found that ~~with the increase of~~as NO_x reduction percentages

increased from 10% to 95%, the simulated O_3 also increased, by a ~~ with the increasing~~ percentage ~~raising~~ rising from ~~within the range of~~ 2% to 78%. ~~This implies~~The implication is that O_3 formation is limited by VOCs in these cases. However, simulated O_3 decreased significantly when the reduction percentage of NO_x increased from 95% to 98%, indicating that O_3 formation switched to the NO_x-limited regime. The dual role~~s~~ of NO_x in O_3 formation ~~are~~ is clearly presented in these experiments.

~~Since~~Because VOCs (particularly AVOCs) and NO_x are generally co-emitted, it is nearly impossible to only reduce VOC emissions ~~with~~ while NO_x remain~~sing~~ unchanged. Therefore, it is vital to find an appropriate ~~cutting~~ reduction ratio of VOCs/NO_x for~~, to~~ effectively controlling O_3 pollution. With the aid of the PBM-MCM model, the net O_3 variations were simulated in the scenarios with different ~~cutting~~ percentage cuts ~~of~~ in VOCs and NO_x, based on the measured VOCs and NO_x. The positive and negative variations indicated increases and decreases of O_3, respectively. ~~Both t~~The percentage cuts in~~cutting percentages of~~ VOCs and NO_x were 0 - 50%~~, with the step of~~at 10% intervals. As shown in Fig. S7, the net O_3 variation increased non-linearly with the increase of percentage cuts in NO_x ~~cutting percentages~~ and decreased with the increase of percentage cuts in VOCs~~ cutting percentages~~. This finding ~~was~~ is consistent with the finding that O_3 formation ~~was~~ occurred in a VOC~~s~~-limited regime during the study period in Wuhan. ~~To~~ For reducing~~e~~ O_3 production, the percentage cut~~sting percentages of~~in VOCs and NO_x ~~could only be accepted~~were only considered acceptable when ~~the~~ O_3 variations were nil or negative. According to Fig. S7, with the increase of ~~cutting~~ percentage cuts in~~s of~~ VOCs from 10.0% to 50.0%, the maximum ~~cutting~~ percentage cut in~~s of~~ NO_x for nil O_3 increment increased from 13.7% to 51.0%, and the ratio of the VOCs percentage cut ~~cutting percentage~~ to NO_x percentage cut ~~cutting percentage~~ (termed the ~~as~~ "VOCs/NO_x cutting ratio") increased from 0.73 to 0.98. Therefore, to maintain a nil/negative O_3 increment, the VOCs/NO_x cutting ratio should be higher than 0.73, given that VOCs were cut by 10% - 50%. This finding could guide the formulation and implementation of effective O_3 control strategies in Wuhan.

Formatted: Highlight

4. Conclusions

In this study, ~~the~~ continuously measured data of speciated VOCs, trace gases, and meteorological parameters in August 2016 at an urban site in Wuhan were analyzed to explore the different characteristics of VOC and O_3 pollution between high-O_3 and non-high-O_3 days. Results indicated that ~~the~~ high temperature, low wind speed, low relative humidity, tropical cyclones, and transport of polluted air masses from northern China to Wuhan were favorable for the occurrence of high-O_3 days during the study period. During high-O_3 days, the mixing ratios of O_3, CO, and TVOCs were 61.2 ± 7.4, 987.8 ± 95.4 and 43.9 ± 3.8 ppbv, about 40%, 37%, and 33% higher than ~~those~~ during non-high-O_3 days (p<0.01), respectively. However, the levels of NO (ΔNO: ~1 ppbv) and NO_2 (ΔNO_2: ~2 ppbv) were comparable between high-O_3 and non-high-O_3 days (p>0.05).

Seven VOC~~s~~ sources were identified: ~~,~~ ~~including~~ gasoline exhaust, diesel and CNG exhausts, stationary combustion, petrochemical industry, solvent usage in painting, asphalt application, and BVOCs. Vehicle exhausts (i.e., gasoline exhaust, diesel and CNG exhausts) made the largest contribution to VOC~~s~~ and O_3 production during both high-O_3 days (45.4 ± 5.2%) and non-high-O_3 days (37.3 ± 2.9%). The contributions of vehicle exhausts and stationary combustion to VOC~~s~~ and O_3 production increased remarkably from non-high-O_3 days to high-O_3 days, suggesting that these sources were the culprit ~~of~~ for elevated O_3 during high-O_3 days. Ozone simulation ~~by~~ using the WRF-CMAQ model indicated that while local formation (74.7 ± 5.8%) accounted for most of the daytime O_3, the nighttime O_3 was significantly elevated by regional transport (59.1 ± 9.9%). As indicated by the relationship between O_3 and its precursors, O_3 formation in urban Wuhan was VOC-limited, and the sensitivity of O_3 formation to AVOCs predominated over BVOCs and CO. To effectively control O_3 pollution, the reduction ratio between VOCs and NO_x should be higher than 0.73. In addition, ~~since~~because VOCs emitted from vehicle exhausts were the main contributors to O_3 production, it is urgent and ~~efficient~~ effective to control vehicle emissions ~~in order to~~to pursue O_3 ~~attainment~~ reduction in Wuhan. This study fill~~ed~~ the knowledge gap ~~of~~ concerning the causes of high O_3 events in Central China, particularly the characterization of local and regional contributions to ~~the~~ high O_3, which ~~would~~ will be of help for O_3 study and control in

other subtropical regions with moist monsoon climates.

Acknowledgements

This study was supported by the National Key R&D Program of China via grant No. 2017YFC0212000, the Wuhan Environmental Monitoring Center via grant No. 250000975, and The Hong Kong Polytechnic University joint supervision scheme with the Chinese mainland, Taiwan and Macao Universities (project No: G-SB63). We ~~were~~ are grateful to the Research Grants Council of Hong Kong for its financial support via grants CRF/C5004-15E, PolyU152052/14E, PolyU152052/16E, and CRF/C5022-14G.

References

An, J.L., Wang, Y.S., Wu, F.K., Zhu, B., 2012. Characterizations of volatile organic compounds during high ozone episodes in Beijing, China. Environ. Monit. Assess. 184, 1879–1889. doi:10.1007/s10661-011-2086-7

Cardelino, C.A., Chameides, W.L., 1995. An observation-based model for analyzing ozone precursor relationships in the urban atmosphere. J. Air Waste Manage. Assoc. 45, 161–180. doi:10.1080/10473289.1995.10467356

Carter, W.P.L., 1994. Development of ozone reactivity scales for volatile organic compounds. Air Waste 44, 881–899. doi:10.1080/1073161X.1994.10467290

Chen, X., Liu, Y., Lai, A., Han, S., Fan, Q., Wang, X., Ling, Z., Huang, F., Fan, S., 2018. Factors dominating 3-dimensional ozone distribution during high tropospheric ozone period. Environ. Pollut. 232, 55–64. doi:10.1016/j.envpol.2017.09.017

Cheng, H.R., Saunders, S.M., Guo, H., Louie, P.K.K., Jiang, F., 2013. Photochemical trajectory modeling of ozone concentrations in Hong Kong. Environ. Pollut. 180, 101–110. doi:10.1016/j.envpol.2013.04.039

Feng, T., Bei, N., Huang, R.J., Cao, J., Zhang, Q., Zhou, W., Tie, X., Liu, S., Zhang, T., Su, X., Lei, W., Molina, L.T., Li, G., 2016. Summertime ozone formation in Xi'an and surrounding areas, China. Atmos. Chem. Phys. 16, 4323–4342. doi:10.5194/acp-16-4323-2016

Gao, J., Zhu, B., Xiao, H., Kang, H., Hou, X., Shao, P., 2016. A case study of surface ozone source apportionment during a high concentration episode, under frequent shifting wind conditions over the Yangtze River Delta, China. Sci. Total Environ. 544, 853–863. doi:10.1016/j.scitotenv.2015.12.039

Gao, J., Zhu, B., Xiao, H., Kang, H., Hou, X., Yin, Y., Zhang, L., Miao, Q., 2017. Diurnal variations and source apportionment of ozone at the summit of Mount Huang, a rural site in Eastern China. Environ. Pollut. 222, 513–522. doi:10.1016/j.envpol.2016.11.031

Gao, W., Tie, X., Xu, J., Huang, R., Mao, X., Zhou, G., Chang, L., 2017. Long-term trend of O_3 in a mega City (Shanghai), China: Characteristics, causes, and interactions with precursors.

Formatted: French (France)

Formatted: French (France)

Sci. Total Environ. 603–604, 425–433. doi:10.1016/j.scitotenv.2017.06.099

Geng, F., Zhang, Q., Tie, X., Huang, M., Ma, X., Deng, Z., Yu, Q., Quan, J., Zhao, C., 2009. Aircraft measurements of O_3, NO_x, CO, VOCs, and SO_2 in the Yangtze River Delta region. Atmos. Environ. 43, 584–593. doi:10.1016/j.atmosenv.2008.10.021

Geng, F., Zhao, C., Tang, X., Lu, G., Tie, X., 2007. Analysis of ozone and VOCs measured in Shanghai: A case study. Atmos. Environ. 41, 989–1001. doi:10.1016/j.atmosenv.2006.09.023

Guenther, A., Karl, T., Harley, P., Wiedinmyer~~t~~, C., Palmer, P.I., Geron, C., 2006. Estimates of global terrestrial isoprene emissions using MEGAN (Model of Emissions of Gases and Aerosols from Nature). Atmos. Chem. Phys. 6, 3181–3210.

Guo, H., Ling, Z.H., Cheung, K., Jiang, F., Wang, D.W., Simpson, I.J., Barletta, B., Meinardi, S., Wang, T.J., Wang, X.M., Saunders, S.M., Blake, D.R., 2013. Characterization of photochemical pollution at different elevations in mountainous areas in Hong Kong. Atmos. Chem. Phys. 13, 3881–3898. doi:10.5194/acp-13-3881-2013

Guo, H., So, K.L., Simpson, I.J., Barletta, B., Meinardi, S., Blake, D.R., 2007. C_1–C_8 volatile organic compounds in the atmosphere of Hong Kong: Overview of atmospheric processing and source apportionment. Atmos. Environ. 41, 1456–1472. doi:10.1016/j.atmosenv.2006.10.011

Han, S.Q., Zhang, M., Zhao, C.S., Lu, X.Q., Ran, L., Han, M., Li, P.Y., Li, X.J., 2013. Differences in ozone photochemical characteristics between the megacity Tianjin and its rural surroundings. Atmos. Environ. 79, 209–216. doi:10.1016/j.atmosenv.2013.06.045

He, K., 2012. Multi-resolution Emission Inventory for China (MEIC): M~~m~~odel framework and 1990-2010 anthropogenic emissions, in: AGU Fall Meeting 2012. Abstract ID: A32B-05. ~~[Please give full citation information.]~~ 2012AGUFM.A32B.05H.

Jia, C., Mao, X., Huang, T., Liang, X., Wang, Y., Shen, Y., Jiang, W., Wang, H., Bai, Z., Ma, M., Yu, Z., Ma, J., Gao, H., 2016. Non-methane hydrocarbons (NMHCs) and their contribution to ozone formation potential in a petrochemical industrialized city, ~~,~~ Northwest China. Atmos. Res. 169, 225–236. doi:10.1016/j.atmosres.2015.10.006

Jiang, F., Guo, H., Wang, T.J., Cheng, H.R., Wang, X.M., Simpson, I.J., Ding, A.J., Saunders, S.M., Lam, S.H.M., Blake, D.R., 2010. An ozone episode in the Pearl River Delta: Field observation and model simulation. J. Geophys. Res. Atmos. 115, 1–18. doi:10.1029/2009JD013583

Jiang, F., Wang, T., Wang, T., Xie, M., Zhao, H., 2008. Numerical modeling of a continuous photochemical pollution episode in Hong Kong using WRF-chem. Atmos. Environ. 42, 8717–8727. doi:10.1016/j.atmosenv.2008.08.034

Jin, X., Fiore, A.M., Murray, L.T., Valin, L.C., Lamsal, L.N., Duncan, B., Folkert Boersma, K., De Smedt, I., Abad, G.G., Chance, K., Tonnesen, G.S., 2017. Evaluating a space-based indicator of surface ozone-NOx-VOC sensitivity over midlatitude source regions and application to decadal trends. J. Geophys. Res. Atmos. 122, 10439–10461. doi:10.1002/2017JD026720

Krupa, S. V, Manning, W.J., 1988. Atmospheric ozone: Formation and effects on vegetation.

Formatted: French (France)

Formatted: French (France)

Formatted: Highlight

Environ. Pollut. 50, 101–137. doi:10.1016/0269-7491(88)90187-X
Kumar, A., Singh, D., Anandam, K., Kumar, K., Jain, V.K., 2017. Dynamic interaction of trace gases (VOCs, ozone, and NOx) in the rural atmosphere of sub-tropical India. Air Qual. Atmos. Heal. 10, 885–896. doi:10.1007/s11869-017-0478-8
Lam, S.H.M., Saunders, S.M., Guo, H., Ling, Z.H., Jiang, F., Wang, X.M., Wang, T.J., 2013. Modelling VOC source impacts on high ozone episode days observed at a mountain summit in Hong Kong under the influence of mountain-valley breezes. Atmos. Environ. 81, 166–176. doi:10.1016/j.atmosenv.2013.08.060
Li, J., Xie, S.D., Zeng, L.M., Li, L.Y., Li, Y.Q., Wu, R.R., 2015. Characterization of ambient volatile organic compounds and their sources in Beijing, before, during, and after Asia-Pacific Economic Cooperation China 2014. Atmos. Chem. Phys. 15, 7945–7959. doi:10.5194/acp-15-7945-2015
Li, L., Chen, C.H., Huang, C., Huang, H.Y., Zhang, G.F., Wang, Y.J., Wang, H.L., Lou, S.R., Qiao, L.P., Zhou, M., Chen, M.H., Chen, Y.R., Streets, D.G., Fu, J.S., Jang, C.J., 2012. Process analysis of regional ozone formation over the Yangtze River Delta, China using the Community Multi-scale Air Quality modeling system. Atmos. Chem. Phys. 12, 10971–10987. doi:10.5194/acp-12-10971-2012
Lin, M., Horowitz, L.W., Payton, R., Fiore, A.M., Tonnesen, G., 2017. US surface ozone trends and extremes from 1980 to 2014: Quantifying the roles of rising Asian emissions, domestic controls, wildfires, and climate. Atmos. Chem. Phys. 17, 2943–2970. doi:10.5194/acp-17-2943-2017
Lin, X., Trainer, M., Liu, S.C., 1988. On the nonlinearity of the tropospheric ozone production. J. Geophys. Res. 93, 15879. doi:10.1029/JD093iD12p15879
Ling, Z.H., Guo, H., 2014. Contribution of VOC sources to photochemical ozone formation and its control policy implication in Hong Kong. Environ. Sci. Policy 38, 180–191. doi:10.1016/j.envsci.2013.12.004
Ling, Z.H., Guo, H., Lam, S.H.M., Saunders, S.M., Wang, T., 2014. Atmospheric photochemical reactivity and ozone production at two sites in Hong Kong: Application of a Master Chemical Mechanism-photochemical box model. J. Geophys. Res. Atmos. 119, 10567–10582. doi:10.1002/2014JD021794
Ling, Z.H., Guo, H., Zheng, J.Y., Louie, P.K.K., Cheng, H.R., Jiang, F., Cheung, K., Wong, L.C., Feng, X.Q., 2013. Establishing a conceptual model for photochemical ozone pollution in subtropical Hong Kong. Atmos. Environ. 76, 208–220. doi:10.1016/j.atmosenv.2012.09.051
Liu, Y., Shao, M., Zhang, J., Fu, L.L., Lu, S.H., 2005. Distributions and source apportionment of ambient volatile organic compounds in Beijing city, China. J. Environ. Sci. Heal. Part A a– Toxic/Hazardous Subst. Environ. Eng. 40, 1843–1860. doi:10.1080/10934520500182842
Logan, J.A., 1985. Tropospheric ozone: Seasonal behavior, trends, and anthropogenic influence. J. Geophys. Res. Atmos. 90, 10463–10482. doi:10.1029/JD090iD06p10463
Lyu, X.P., Chen, N., Guo, H., Zhang, W.H., Wang, N., Wang, Y., Liu, M., 2016. Ambient volatile organic compounds and their effect on ozone production in Wuhan, central China.

Formatted: French (France)

Formatted: French (France)

Formatted: French (France)

Sci. Total Environ. 541, 200–209. doi:10.1016/j.scitotenv.2015.09.093
Lyu, X.P., Guo, H., Simpson, I.J., Meinardi, S., Louie, P.K.K., Ling, Z., Wang, Y., Liu, M., Luk, C.W.Y., Wang, N., Blake, D.R., 2016a. Effectiveness of replacing catalytic converters in LPG-fueled vehicles in Hong Kong. Atmos. Chem. Phys. 16, 6609–6626. doi:10.5194/acp-16-6609-2016
Lyu, X.P., Liu, M., Guo, H., Ling, Z.H., Wang, Y., Louie, P.K.K.K., Luk, C.W.Y.Y., 2016b. Spatiotemporal variation of ozone precursors and ozone formation in Hong Kong: Grid field measurement and modelling study. Sci. Total Environ. 569–570, 1341–1349. doi:http://dx.doi.org/10.1016/j.scitotenv.2016.06.214
McDonald, B.C., De Gouw, J.A., Gilman, J.B., Jathar, S.H., Akherati, A., Cappa, C.D., Jimenez, J.L., Lee-Taylor, J., Hayes, P.L., McKeen, S.A., Cui, Y.Y., Kim, S.W., Gentner, D.R., Isaacman-VanWertz, G., Goldstein, A.H., Harley, R.A., Frost, G.J., Roberts, J.M., Ryerson, T.B., Trainer, M., 2018. Volatile chemical products emerging as largest petrochemical source of urban organic emissions. Science. 359, 760–764. doi:10.1126/science.aaq0524
Monks, P.S., 2005. Gas-phase radical chemistry in the troposphere. Chem. Soc. Rev. 34, 376. doi:10.1039/b307982c
Monks, P.S., Archibald, A.T., Colette, A., Cooper, O., Coyle, M., Derwent, R., Fowler, D., Granier, C., Law, K.S., Mills, G.E., Stevenson, D.S., Tarasova, O., Thouret, V., Von Schneidemesser, E., Sommariva, R., Wild, O., Williams, M.L., 2015. Tropospheric ozone and its precursors from the urban to the global scale from air quality to short-lived climate forcer. Atmos. Chem. Phys. 15, 8889–8973. doi:10.5194/acp-15-8889-2015
Paatero, P., 1997. Least squares formulation of robust non-negative factor analysis. Chemom. Intell. Lab. Syst. 37, 23–35. doi:10.1016/S0169-7439(96)00044-5
Paatero, P., Tapper, U., 1994. Positive matrix factorization: A~~a~~ non-negative factor model with optimal utilization of error estimates of data values. Environmetrics 5, 111–126. doi:10.1002/env.3170050203
Pan, X., Kanaya, Y., Tanimoto, H., Inomata, S., Wang, Z., Kudo, S., Uno, I., 2015. Examining the major contributors of ozone pollution in a rural area of the Yangtze River Delta region during harvest season. Atmos. Chem. Phys. 15, 6101–6111. doi:10.5194/acp-15-6101-2015
Roelofs, G.J., Lelieveld, J., 1997. Model study of the influence of cross-tropopause O3 transports on tropospheric O3 levels. Tellus B Chem. Phys. Meteorol. 49, 38–55. doi:10.3402/tellusb.v49i1.15949
Shao, P., An, J., Xin, J., Wu, F., Wang, J., Ji, D., Wang, Y., 2016. Source apportionment of VOCs and the contribution to photochemical ozone formation during summer in the typical industrial area in the Yangtze River Delta, China. Atmos. Res. doi:10.1016/j.atmosres.2016.02.015
Sharkey, T.D., Wiberley, A.E., Donohue, A.R., 2008. Isoprene emission from plants: Why and how. Ann. Bot. 101, 5–18. doi:10.1093/aob/mcm240
So, K.L., Wang, T., 2003. On the local and regional influence on ground-level ozone concentrations in Hong Kong. Environ. Pollut. 123, 307–317. doi:10.1016/s0269-7491(02)00370-6

Formatted: French (France)

Stevenson, D.S., Young, P.J., Naik, V., Lamarque, J.F., Shindell, D.T., Voulgarakis, A., Skeie, R.B., Dalsoren, S.B., Myhre, G., Berntsen, T.K., Folberth, G.A., Rumbold, S.T., Collins, W.J., MacKenzie, I.A., Doherty, R.M., Zeng, G., Van Noije, T.P.C., Strunk, A., Bergmann, D., Cameron-Smith, P., Plummer, D.A., Strode, S.A., Horowitz, L., Lee, Y.H., Szopa, S., Sudo, K., Nagashima, T., Josse, B., Cionni, I., Righi, M., Eyring, V., Conley, A., Bowman, K.W., Wild, O., Archibald, A., 2013. Tropospheric ozone changes, radiative forcing and attribution to emissions in the Atmospheric Chemistry and Climate Model Intercomparison Project (ACCMIP). Atmos. Chem. Phys. 13, 3063–3085. doi:10.5194/acp-13-3063-2013

Tilton, B.E., 1989. Health effects of tropospheric ozone. Environ. Sci. Technol. 23, 257–263. doi:10.1021/es00180a002

Verstraeten, W.W., Neu, J.L., Williams, J.E., Bowman, K.W., Worden, J.R., Boersma, K.F., 2015. Rapid increases in tropospheric ozone production and export from China. Nat. Geosci. 8, 690–695. doi:10.1038/ngeo2493

Wang, N., Guo, H., Jiang, F., Ling, Z.H., Wang, T., 2015. Simulation of ozone formation at different elevations in mountainous area of Hong Kong using WRF-CMAQ model. Sci. Total Environ. 505, 939–951. doi:10.1016/j.scitotenv.2014.10.070

Wang, Q., Han, Z., Wang, T., Zhang, R., 2008. Impacts of biogenic emissions of VOC and NO_x on tropospheric ozone during summertime in eastern China. Sci. Total Environ. 395, 41–49. doi:10.1016/j.scitotenv.2008.01.059

Wang, T., Nie, W., Gao, J., Xue, L.K., Gao, X.M., Wang, X.F., Qiu, J., Poon, C.N., Meinardi, S., Blake, D., Wang, S.L., Ding, A.J., Chai, F.H., Zhang, Q.Z., Wang, W.X., 2010. Air quality during the 2008 Beijing Olympics: Secondary pollutants and regional impact. Atmos. Chem. Phys. 10, 7603–7615. doi:10.5194/acp-10-7603-2010

Wang, T., Wei, X.L., Ding, A.J., Poon, C.N., Lam, K.S., Li, Y.S., Chan, L.Y., Anson, M., 2009. Increasing surface ozone concentrations in the background atmosphere of Southern China, 1994-2007. Atmos. Chem. Phys. 9, 6217–6227. doi:10.5194/acp-9-6217-2009

Wang, T., Xue, L., Brimblecombe, P., Lam, Y.F., Li, L., Zhang, L., 2016. Ozone pollution in China: A review of concentrations, meteorological influences, chemical precursors, and effects. Sci. Total Environ. 575, 1582–1596. doi:10.1016/j.scitotenv.2016.10.081

Wang, Y., Guo, H., Zou, S.C., Lyu, X.P., Ling, Z.H., Cheng, H.R., Zeren, Y., 2018. Surface O_3 photochemistry over the South China Sea: Application of a near-explicit chemical mechanism box model. Environ. Pollut. 234, 155–166. doi:10.1016/j.envpol.2017.11.001

Wang, Y., Wang, H., Guo, H., Lyu, X.P., Cheng, H.R., Ling, Z.H., Louie, P.K.K., Simpson, I.J., Meinardi, S., Blake, D.R., 2017. Long term O3-precursor relationships in Hong Kong: Field observation and model simulation. Atmos. Chem. Phys. Discuss. 1–29. doi:10.5194/acp-2017-235

Xu, Z., Huang, X., Nie, W., Chi, X., Xu, Z., Zheng, L., Sun, P., Ding, A., 2017. Influence of synoptic condition and holiday effects on VOCs and ozone production in the Yangtze River Delta region, China. Atmos. Environ. 168, 112–124. doi:10.1016/j.atmosenv.2017.08.035

Xu, Z., Xue, L., Wang, T., Xia, T., Gao, Y., Louie, P.K.K., Luk, C.W.Y., 2015. Measurements of peroxyacetyl nitrate at a background site in the Pearl River Delta region: production

Formatted: French (France)

Formatted: French (France)

efficiency and regional transport. Aerosol Air Qual. Res. 15, 833–841. doi:10.4209/aaqr.2014.11.0275

Xue, L.K., Wang, T., Gao, J., Ding, A.J., Zhou, X.H., Blake, D.R., Wang, X.F., Saunders, S.M., Fan, S.J., Zuo, H.C., Zhang, Q.Z., Wang, W.X., 2014. Ground-level ozone in four Chinese cities: Pprecursors, regional transport and heterogeneous processes. Atmos. Chem. Phys. 14, 13175–13188. doi:10.5194/acp-14-13175-2014

Yuan, B., Shao, M., Lu, S., Wang, B., 2010. Source profiles of volatile organic compounds associated with solvent use in Beijing, China. Atmos. Environ. 44, 1919–1926. doi:10.1016/j.atmosenv.2010.02.014

Yuan, Z., Lau, A.K.H., Shao, M., Louie, P.K.K., Liu, S.C., Zhu, T., 2009. Source analysis of volatile organic compounds by positive matrix factorization in urban and rural environments in Beijing. J. Geophys. Res. 114. doi:10.1029/2008jd011190

Zhang, J., Wang, T., Chameides, W.L., Cardelino, C., Kwok, J., Blake, D.R., Ding, A., So, K.L., 2006. Ozone production and hydrocarbon reactivity in Hong Kong, Southern China. Atmos. Chem. Phys. Discuss. 6, 8961–9002. doi:10.5194/acpd-6-8961-2006